



# A Fluid Structure Interaction Analysis of Vertical-Lift-Producing Daggerboards

Casey Brown and Cody Stansky  
Glen Cove, NY

A thesis submitted in partial fulfillment of the requirements for the Bachelor of Science Degree in Naval Architecture and Marine-Engineering

## 1 ABSTRACT

This thesis analyses the steady state fluid structure interactions, FSI, of high-performance sailing hydrofoils. This was performed by evaluating an isotropic, CV-style sailing hydrofoil, similar to those being used on the AC 50's, which will be competing in the 2017 Americas Cup. The FSI analysis was completed using the multi-physics simulation software, StarCCM+. The results from the FSI study are compared to a CFD analysis of the un-deformed foil, to determine the value of the FSI study. The deformed foil performance varied significantly enough at speeds of 30 knots and above to warrant a FSI study.

## 2 NOMENCLATURE

CFD	Computational Fluid Dynamics
FSI	Fluid Structure Interaction
FEA	Finite Element Analysis
FEM	Finite Element Method
RANS	Reynolds Average Navier Stokes
$c$	Foil Chord length
$i$	Fluid Internal Energy
UFS	Free Stream Velocity
T	Temperature
$\nabla$	Dell Operator
$V_\infty$	Free Stream Velocity
$u$	Longitudinal Component of Velocity
$v$	Transverse Component of Velocity
$w$	Vertical Component of Velocity, Downwash Velocity
$k$	Thermal Conductivity
$g$	Acceleration Due to Gravity
$p$	Fluid Absolute Pressure
Star-CCM+	Viscous CFD Program
$C_d$	Drag Coefficient
$C_l$	Lift Coefficient
$L'$	Lift per Unit Span

$D'$	Drag per Unit Span
$\Gamma$	Circulation
$\mu$	Fluid Dynamic Viscosity
$\nu$	Fluid Kinematic Viscosity
$\rho$	Fluid Density
$\sigma_{ij}$	Normal Stress on I <sup>th</sup> Face in J <sup>th</sup> Direction
$\tau_{ij}$	Shear Stress on I <sup>th</sup> Face in J <sup>th</sup> Direction
$\phi$	Viscous Dissipation

## 3 INTRODUCTION

The lack in market scale and a low budget ceiling often force designers to make compromises in their design process. The challenging aspect of limited funding is deciding what areas of the design can be simplified, while still maintaining a safe and high-quality product. This thesis project examines the value of Fluid Structure Interaction (FSI) analysis, with a focus on sailing hydrofoils. FSI is a computationally expensive, iterative process that, in this case, analyzes the forces imparted on a foil by a moving flow field, then examines the deflection of the foil from the calculated pressure and shear forces; it repeats these processes until the deflection and forces converge to a steady-state equilibrium.

Hydrofoils provide vertical lift, to raise racing sailboat hulls clear of the water, greatly reducing drag. Since hydrofoils support the entire weight of the boat, along with the forces induced by the sails, they are a prime candidate for consideration in the FSI analysis process. The CV hydrofoil is recognized as the standard for today's leading edge racing catamaran designs. In addition, when discussing this topic with industry professionals, it became apparent that leading designers are considering a variety of implementations of FSI, especially at the highest level of sailing design, the America's Cup.

## 4 BACKGROUND

### 4.1 VERTICAL-LIFT-PRODUCING DAGGERBOARDS

A recent development in yacht design is the addition of a horizontal wing element on daggerboards to help produce vertical lift, while simultaneously providing the required side force. The advantage of this type of arrangement is the effective reduction in displacement, and subsequent reduction of resistance, because of the vertical lift produced by the daggerboard. This horizontal wing element can also significantly increase heave stability, even when a minimal amount of vertical lift is being generated.



Figure 1. ORMA 60 with lifting foils  
Source: Charterworld.com

### 4.2 LIFTING FOIL PROFILES

Lifting foils have developed increasingly complex shapes since their first generation, as constant-curvature foils. All of these variations are aimed at providing a solution that produces vertical lift, while still resisting side force in stable manner. Although the foil planform and section are important in the overall design of the foil, both attributes vary little in comparison to the foil profile. The profile of the foil is defined as the projection of the foil onto a plane normal to the free stream vector, at zero angle of attack. It is common to relate the shape of these different profiles to letters of the alphabet. For example, a constant-curvature-lifting foil, as shown above on the ORMA 60, can be referred to as a C foil.

The C-L Foil and its derivatives (Figure 2) have proven to be the most popular. This combination provides heave stability of the acute L configuration with the added benefit of the lift vectoring of the C profile. This setup does lower the righting moment produced by the foil. The righting moment can be improved by adding a point of inflection in the strut of the foil, but this adds complexity to the daggerboard case. Because of its simplicity, as compared to a foil with an inflection point, the C-L foil is

the most popular configuration and will be used for our analysis.

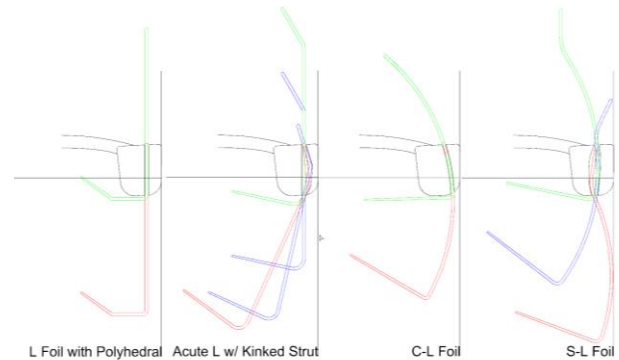


Figure 2. C-L and S-L lifting foils

### 4.3 DESIGN CONSIDERATIONS

Traditionally, designers have only had to design daggerboards and the required supporting structure to endure the lateral force produced by the sails, sideforce. However, the addition of a vertical force component, which is often much larger than the sideforce, presents significant design challenges. The additional lifting force not only complicates the design and construction of the foil, but also effects the control systems and supporting structure.

#### 4.3.1 Stability

The stability of a foil is just as important as the foils ability to efficiently produce lift. Lifting foils must be able to produce constant vertical lift while varying speed, leeway angle, pitch angle, heel angle and immersion ratio. The ability to provide constant lift is referred to as heave stability. In addition to heave stability, the lifting foil should also provide some resistance to heel. Modification to foil geometry, in order to improve roll stability, will often result in an increase in drag. This reduction of the lift to drag ratio is often necessary to produce a foil that can be used effectively in a racing environment. Although a low drag foil design will produce high peak speeds, a more stable foil design, that is less likely to stall when experiencing minor disturbances, will be able to maintain a higher average speed.

#### 4.3.2 Operation

A modern lifting foil is subject to significant hydrodynamic loading. In addition to the stresses experienced during steady state operation, lifting foils are also exposed to significant dynamic loading conditions while maneuvering. The addition of dynamic loads often results in the highest deflections seen by a lifting foil under normal operation. Large deformation of the foil structure may negatively impact the hydrodynamic performance of the foil and in some cases, contribute to stall. This is why

it is critical to be able to predict and account for these deflections in the design of a lifting foil.

#### 4.4 WHY FSI?

To date, nearly all published work related to the performance of lifting foils assumes a rigid structure. This greatly simplifies the analysis and still provides a reasonably accurate solution provided structural displacements are small, however, variety of hydrodynamic issues could significantly affect the performance of a flexible daggerboard. Physical conditions such as flutter and cavitation can greatly reduce foil efficiency and may be overlooked without a full FSI analysis.

### 5 THEORY

#### 5.1 TWO-DIMENSIONAL FOIL CONCEPT

The characteristics of a wing, or in this case hydrofoil, may be largely predicted using two-dimensional theory as long as the span is long with respect to the chord, the mach number remains below the subcritical level, and the chordwise velocity is much more significant than the spanwise flow (Abbott, 1959). The sailing hydrofoil satisfies the three prior mention criteria. Abbott and von Doenhoff use linear theory to detail two-dimensional foil characteristics based on dimensionless lift and drag coefficients for various foil geometries, and angles of attack. The force-per-unit-span values of lift and drag are given by the following expressions:

$$L' = C_l \frac{1}{2} \rho V_\infty^2 c \quad (1)$$

$$D' = C_d \frac{1}{2} \rho V_\infty^2 c \quad (2)$$

#### 5.2 THREE-DIMENSIONAL FOIL CONCEPT

Two-dimensional, inviscid foil theory can accurately predict lift and drag for a three-dimensional foil with infinite span and a constant foil section up to the point of stall. Obviously, this approach is not fully applicable to the case of sailing hydrofoil design. Variation in plan form area, foil profile, end effects, and twist, among other three-dimensional aspects significantly alter foil performance, and must be accounted for.

##### 5.2.1 Induced drag

The flow at any section in a three-dimensional foil varies from that implied by two-dimensional theory, partially from the effects of the trailing vortices. These vortices induce a vertical component of the fluid flow, the

downwash velocity  $w$ , normal to both the span and the direction of motion, oriented toward the high pressure side of the foil. The impact of this induced flow is to alter the angle of the lift vector towards the drag vector by  $w/V_\infty$ , adding an element of induced drag, see

Figure 3.

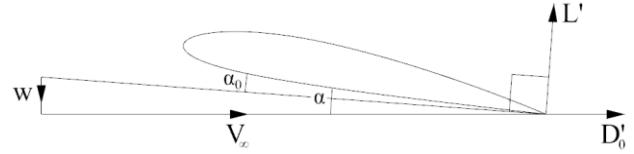


Figure 3: Induced Velocity -

##### 5.2.2 Turbulence

Turbulence is defined as a flow regime characterized by unsteady, stochastic or random property changes in which all three velocity components fluctuate around a mean value. Turbulent flow occurs, in general, at Reynolds numbers above  $5 \times 10^5$  and is extremely influential to foil lift and drag attributes. Turbulent flow is often present close to foil surfaces in the boundary layer. A flow with a turbulent boundary layer can keep the flow attached over a larger percentage of the chord, delaying separation, and thus decreasing pressure drag, at the cost of an increase in skin friction drag. For NACA 6-series foils pressure drag is always smaller than friction drag, so laminar flow is ideal.

#### 5.3 COMPUTATIONAL FLUID DYNAMICS

Three main principles are known to govern fluid dynamics: conservation of mass, conservation of momentum, and conservation of energy. Computational Fluid Dynamic programs solve the RANS equations by applying the above numerically in order to model fluid flow. Star-CCM+ contains a RANSE CFD code that includes the viscosity and vorticity effects neglected by potential flow, a less computationally expensive CFD code.

##### 5.3.1 Reynolds Averaged Navier Stokes Equations

The conservation equations for momentum and mass can be combined and averaged to form the following equation used to solve CFD simulations.

$$\rho \left[ \frac{\partial \bar{u}_i}{\partial t} + \bar{u}_j \frac{\partial \bar{u}_i}{\partial x_j} \right] = \rho \bar{g} + \frac{\partial}{\partial x_j} \left[ \frac{\partial \bar{p}}{\partial x_i} + \mu \left( \frac{\partial \bar{u}_i}{\partial x_j} + \frac{\partial \bar{u}_j}{\partial x_i} \right) - \rho \overline{u_i' u_j'} \right] \quad (3)$$

The final three terms, on the right side of the equation, include the pressure gradient, shear stress, and

Reynolds stress respectively. Potential flow neglects both shear stress and Reynolds stress and must account for these effects using empirical corrections.

### 5.3.2 Energy Equation

This physical principal is equivalent to the first law of thermodynamics, which dictates that energy is always conserved. Applying this law to fluid flow, the rate of change of energy inside the element must equal the sum of the net flux of heat into the element, and the rate of work done on the element, from body and surface forces; this law is given by the following equation:

$$\frac{\partial(\rho i)}{\partial t} + \nabla \cdot (\rho i \vec{V}) = -p(\nabla \cdot \vec{V}) + \nabla \cdot (k \nabla T) + \varphi \quad (4)$$

where  $i$  is the internal energy,  $p$  is the absolute pressure,  $k$  is the thermal conductivity,  $T$  is the temperature, and  $\varphi$  is the viscous dissipation term. These two depicted equations, derived from the three classical laws of fluid dynamics, are the core of a RANSE fluid flow solver.

### 5.3.3 RANSE Turbulence Models

The numerical discretization of the RANSE requires the use of turbulence models in order to achieve a reasonable computational speed, as the turbulent boundary layer is characterized by unsteady fluctuations. The goal of turbulence modeling is to predict the velocity, pressure, and temperature field without the need to model the entire turbulent flow region (Fast, 2014). This process is achieved through the use of turbulent models offered within various RANS CFD programs. Common models include  $k-\varepsilon$ ,  $k-\omega$ , and  $SST k-\omega$ . The  $k-\varepsilon$  model uses a kinetic energy approach and adds relatively little to the computational power required, but does have some shortcomings in more turbulent flows. The  $k-\omega$  model makes use of the transport theorem to apply a specific dissipation rate to the flow, however it can require significant additional computing power. The  $SST k-\omega$  model is a combination of both, implementing the  $k-\omega$  model in turbulent boundary layer areas and the  $k-\varepsilon$  model farther from typical turbulent regions (Fast, 2014).

### 5.3.4 Turbulent Boundary Layer

The boundary layer, is considered to be the thin region near the surface of a body where viscous effects are significant. This layer is necessary for the flow to transition from the free stream velocity outside of the boundary layer to a velocity of zero at the wall. This region is governed by the assumptions that fluid velocity normal to the surface is much less than fluid velocity parallel to the surface, and that the velocity gradient normal to the surface is much higher than that parallel to the surface.

Although both laminar and turbulent boundary layer flows share these characteristics, the latter will develop three distinct regions (Figure 4); these include the viscous sublayer, the buffer layer, and the fully turbulent region. The boundary layer characteristics can be described with a near wall Reynolds number  $y^+$  that is a function of the friction velocity, see equation  $y^+ = \frac{y^* u_t}{\nu}$  (5).

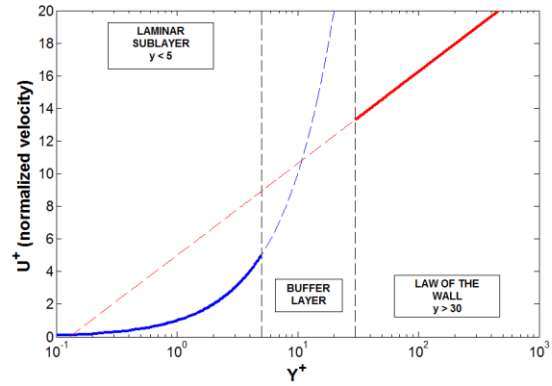


Figure 4 Two-layer zonal approach  
Source: www.computationalfluidynamics.com

$$y^+ = \frac{y^* u_t}{\nu} \quad (5)$$

Traditional CFD methods have used a wall function approach, where the first cell of the mesh must extend past a point where the  $y^+$  value is 50. This approach applies an empirical average without having to precisely solve the viscous sublayer and buffer layer. The two-layer zonal approach explicitly models these near wall flow effects, requiring significant additional computational time. The  $k-\omega$  turbulence model can simulate both the viscous sublayer and the fully turbulent regions. The first mesh cell must have an outer node  $y^+$  value around one, with a series of thin growing prism layers for the first ten cells to the extent of the boundary layer.

### 5.3.5 Boundary Conditions

The previously presented governing equations of CFD apply to all simulations attempted using RANS CFD code. The major difference between the analyses of different physical events lies in the boundary conditions (Anderson 1995). Proper implementation of boundary conditions is necessary in order to attain accurate numerical simulation results. An example of a boundary condition would be a no slip wall, in viscous flow, where the fluid velocity approaches zero velocity at the wall. These conditions are enabled in simulations to approximate realistic conditions.

## 5.4 FINITE ELEMENT ANALYSIS

### 5.4.1 Finite Element Method

The finite element method provides a numerical, piecewise analysis technique for calculating approximate solutions to problems with irregular or complicated geometry, for which no straightforward analytical solution exists. The method discretizes the continuum of a structural problem into series individual nodes linked by elements. Each node, which may be free in up to six degrees of freedom, acts as a boundary condition for a group of elements, at which point the applied equations must be equal. The elements are assigned a interpolation function, based on the field variable being investigated. The stiffness matrices for each element are combined to produce the matrix defining the entire continuum. Boundary conditions are applied to groups of nodes and the continuum is then solved for the unknown field variables at the nodal points. Steady problems can be solved using sets of algebraic equations, while unsteady simulations require ordinary differential equations.

The finite element method has gained significant traction, following the growth of computing power, for all forms of solid stress problems and is now viewed as the dominant numerical method in this field. In structural problems, elements are assigned elastic properties with displacement as the unknown field variable.

## 5.5 FLUID STRUCTURE INTERACTION

The fluid flow characteristics analyzed in CFD and the structural characteristics modeled in FEA both produce results relevant to many engineering designs. Analyzing the two separately provides the beginning of the design framework, however, in many problems the fluid flow can significantly impact the structural response of an object. There are several different methods of FSI intended to examine different physical phenomena. The breadth of this field of study limits us to discussing just those aspects related to foil design, rather than all possible forms here. The term FSI includes all forms of thermo-mechanical interaction between a solid structure and a fluid. In terms of this thesis, it is the study of the transfer of momentum and forces between a fluid region and a solid body. There are many types of interactions that can be combined to form a multitude of different simulations.

### 5.5.1 Dynamic Fluid Body Interaction

One of the most basic versions of FSI is dynamic fluid body interaction, DFBI. This is when a body is fixed in deformation to examine its movement characteristics through a fluid flow, such as the seakeeping of a ship where the bending of the ship is assumed to not impact the seakeeping characteristics.

### 5.5.2 Deformable Structure

A flexible structure can be fixed in rotation and translation, but not in deformation. This allows the structure's response to the fluid flow to be examined. This method is applied to the current study in order to examine the structural response of the foil to the encountered fluid flow. A DFBI study can incorporate a deformable structure such as the case in which a ships structural response in a sea state is examined and correlated to the ships seakeeping characteristics.

### 5.5.3 One-way Interaction

One-way interactions can be applied in cases where the structural response will do little to impact the fluid flow. In this case, the forces exerted or heat transferred from the fluid to the structure are applied to the structure, neglecting the impact of the structure's property changes on the fluid flow. This can also be applied in the opposite manner, for example in a piston and cylinder where the structure impacts the fluid flow, but the flow does little to deform the structure.

### 5.5.4 Two-way Interaction

Two-way interactions encompass a broad range of FSI simulations. In this type of analysis, the pressures and shear forces from the fluid affect the displacement and deformation of the structure, which in turn affects the fluid flow and therefore the pressures and shear forces that the fluid exerts on the structure. Two-way interactions can be both steady and unsteady depending on the FSI aspect being investigated.

### 5.5.5 Weak Coupling

Weak coupling implies that the structural response to the fluid flow is slow. This type of simulation is most often used with stiff structures in compressible flows. Analyses where a steady state response is the target, and the main impacts on fluid flow are from the velocity of the moving structure, are prime candidates for this type of simulation.

### 5.5.6 Strong Coupling

Nearly incompressible flows, encountering relatively flexible objects, require a strong coupling as opposed to a weak one. These simulations see variations in the flow characteristics from the deformation of the structure, even approaching a steady state solution. Strong coupling is an implicit form of coupling that is necessary for most dynamic problems.

### 5.5.7 Steady

Steady state simulations provide a static representation of the impact of fluid flow on a structure, in

an attempt to examine the variation in characteristics a steady state, deformed point.

### 5.5.8 Unsteady

Unsteady simulations are employed to study a variety of dynamic effects. These could include ship motions, flutter in a wing, and other vibrations in a structure.

Table 1 FSI Analysis Summary

Motion Specification	<b>Fixed*</b>
	Free
Structural Response	Rigid
	<b>Deformable*</b>
Coupling Classification	One-Way
	<b>Two-Way*</b>
Coupling Strength	<b>Strong*</b>
	Weak
Time Domain	<b>Steady*</b>
	Unsteady

### 5.5.9 FSI Coupling

There are several different ways to perform an FSI analysis with CAE. The fluid solver can be run in one code and the solid solver in another and through a method of coupling, a FSI analysis can be run. Most CAE software has the ability to perform some type of coupling with other programs but the level of compatibility differs.

The two most relevant types of coupling are file based coupling and co-simulation. File based coupling uses output files to transfer data from one code to another. In this process a CFD solution is run, pressure fields and traction fields from this solution are exported from the CFD code and then imported into the FEA code where they are applied to the FE model as loads. This process can be done manually by the user importing and exporting files, or it can be automated with the use of a script. This type of coupling is classified as a weak coupling and is best suited for a one way FSI analysis as the process of iterating is quite cumbersome.

The second type of coupling is known as co-simulation. The main advantage co-simulation is the frequency at which data exchange occurs. A two-way exchange of data forms a deep level of communication between the solvers that makes it possible to simulate the interactions of different physical phenomena. Co-simulation differs from file based coupling in that the coupling between the two codes is much stronger, the exchange of data between the two solvers is done automatically, and the two solvers run simultaneously. This type of coupling is classified as strong coupling and is best applied to a two way FSI analysis.

## 5.6 COMPUTATIONAL RESOURCES

When solving an engineering problem with the help of CAE, engineers are very often constrained by the computing power available to them. Multi solver simulations can become computationally expensive very quickly, so many engineers avoid larger, non-linear simulations that could provide higher fidelity insight. To avoid compromising the integrity of such results it is necessary tailor the solution to the capabilities of the available resources.

### 5.6.1 High Performance Computing (HPC)

High Performance Computing (HPC) is the use of parallel processing for running advanced applications quickly and efficiently. A decade ago, (HPC) was primarily associated with large supercomputers. Today HPC is available on the entire computer spectrum. More cores per CPU, more and faster memory channels, faster disk storage and faster interconnects have granted wider access of HPC to the general public.

In general, CAE simulation requires large amounts of CPU and RAM to run quickly and efficiently. The number of physical cores and the core clock speed allows trillions of Floating Point Operations (FLOPS) to be performed every second. Modern Intel processors have incorporated an operation called Hyper Threading (HT), which allows the CPU to more evenly distribute the workload among processors. In HT each physical core appears as two virtual cores to the operating system. This increases the number of basic ordered sequences of instructions, threads, that can be passed through a single core hence the term Hyper-Threading.

Although CPU is the main workhorse in performing numerical calculation, the CPU is fed these calculations by the RAM. For this reason, neither CPU clock speed, nor cache size or even system architecture is as significant as the memory system installed when it comes to simulation performance. Without the proper memory system to support it, large amounts of CPU cannot be properly utilized. The two memory characteristics of interest are the number of channels and memory clock speed. This allows the memory system to keep up with the capacity of the CPU.

## 6 PROCEDURE

### 6.1 2D SECTION ANALYSIS

The first step in the design process of a lifting foil is the selection of 2D sections. Analysis of sections in 2D requires much less time and resources than a full 3D analysis, while providing a reasonably accurate prediction of the performance of the lifting foil in the preliminary stage of design.

6.1.1 Hydrodynamic Considerations

From a hydrodynamic standpoint, a section with a high lift to drag ratio and low peak pressure is favorable. A high lift to drag ratio results in lower overall resistance for the lift produced over a range of angles of attack. A lower peak pressure reduces the drag effects caused by separation and cavitation.

In certain operating conditions it is difficult to prevent significant cavitation from occurring. The unsteady dynamic forces and turbulent incident flow experienced by Americas Cup foils make cavitation unavoidable during normal operation. For this reason, some designers have sought out ways to exploit the effects of cavitation. Partial cavitation actually reduces frictional drag, but fluctuations in this area of cavitation usually result in an increase in form drag. Within a range of lift coefficients and cavitation numbers, modifications to the suction side of a section can suppress these oscillations. This can reduce the frictional resistance of the foil section without the typical increase in form drag.

6.1.2 Structural Considerations

Typically, sections considered for high speed applications are very thin. Often it is necessary to thicken the ideal section once structural aspects are considered. Because the 2D analysis is the very beginning of the design process the thickness required to limit structural deflections is hard to quantify at this point. Often the initial section thickness is determined using first principles but this method has its drawbacks, as we will discuss later. Section performance is very sensitive to thickness changes, so the ability to accurately quantify deflections and the subsequent change in performance is critical to the design of a section. This is an example of where a FSI analysis can have significant effects on the overall performance of a lifting foil.

6.1.3 Section Selection

The selection of an appropriate 2D section requires a plethora of design considerations as mentioned above, many of which are dependent on the specific vessel characteristics. In order to most accurately simulate the operating conditions experienced during the operation, it was decided to use a section already tailored to this type of application. Morrelli and Melvin Design and Engineering was kind enough to provide the 3D geometry of a CV foil designed for use on an AC50. The local section at the root of the provided geometry was normalized and extracted for use in the 2D analysis. A summary of section characteristics is presented in Table 2 along with the normalized section in Figure 5.

Table 2 MM AC50 Section Properties

$t_{max}/C$	=0.14
-------------	-------

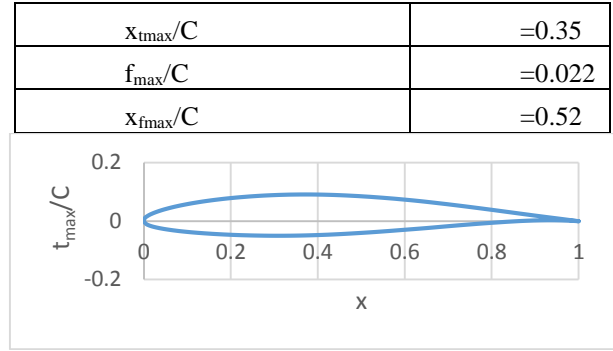


Figure 5. MM AC50 Foil Section

6.1.4 Analysis Limitations

While a 2D analysis is critical to the hydrofoil design process, there are limitations on the results that must be taken into consideration. The most obvious of which is that 2D analysis cannot capture the effects of spanwise flow, which can become significant on complex geometries such as a CV foil. The effects of tip vortices and vortex shedding is not accounted for, as 2D analysis assumes infinite span. These assumptions typically result in an over-prediction of lift/drag characteristics when compared to 3D analysis.

Analysis of this section was performed in XFLR5, a 2D panel code, used for the analysis of airfoil sections at low Reynold Numbers. XFLR5 is simply an open sourced GUI (Graphical User Interface) or “front end” for MIT’s XFOIL code. The code is very robust and has been modified to apply corrections that a typical potential flow analysis would neglect. XFLR5 has the capability to run a corrected viscous and compressible solution, although the models used differ than those used in 3D fluid dynamic simulations.

6.1.5 Analysis Results

The MM AC50 section was tested at three different Reynolds numbers, the same as our 3D testing matrix, over a range of angles of attack. The 2D analysis was performed over a range of  $\alpha$ 's from -1 degrees to an angle of 15 degrees, just below stall. Although our 3D testing matrix will only cover a fraction of this range of  $\alpha$ 's, we can more clearly see overall trends with this full range of angles.

The lift to drag ratio of the foil section, as a function of  $\alpha$ , is shown below in Figure 6. Here we can see the “efficiency” of the section over the full range of operating conditions. There is a pronounced peak in the lift to drag ratios of each Reynolds number at low  $\alpha$ 's. This is where the foil is designed to operate for a given speed. This particular thin section has a high lift to drag ratio, but a relatively low angle of stall, characteristics typical of this application.

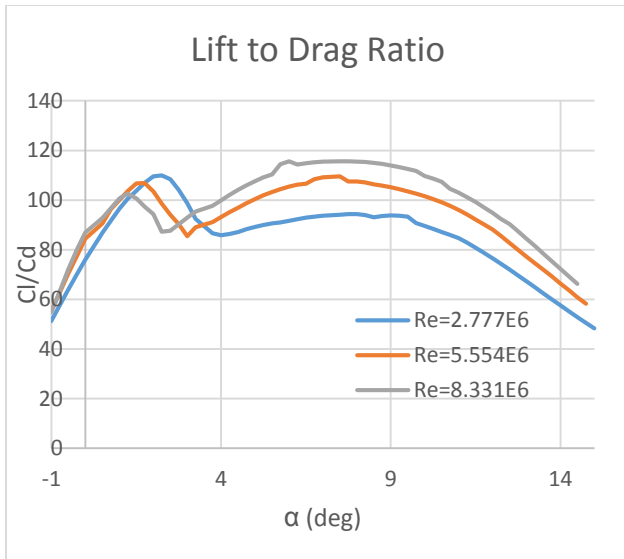


Figure 6 MM AC50 Lift to drag ratio

In addition to providing general section performance information, XFLR5 has the capability to show boundary layer thickness along the length of the chord. As can be seen in Figure 7, the boundary layer is the thickest towards the trailing edge of the suction side of the section. The thickness at this location was used to approximate the region where boundary layer effects need to be considered in the 3D analysis.

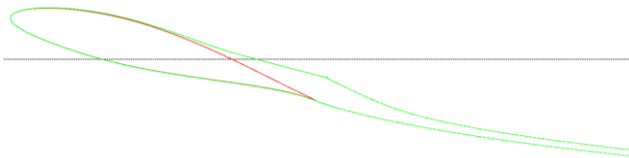


Figure 7 XFLR5 Boundary Layer Output

## 6.2 TEST MATRIX

The Reynolds numbers tested were chosen based on the operating envelope of the geometry provided. A Reynolds number corresponding to fifteen knots was chosen as the low end of our testing matrix to determine the performance of the section at the low end of the foiling envelope. At this point in the operating range we can reasonably assume the vessel is fully foiling and interactions with the hull can be ignored. The upper range of our testing matrix reflects the upper range of speeds experienced by Americas Cup yachts during racing. This is where we can expect the highest deflections and therefore the highest changes in performance.

The 2D results were analyzed to determine the set of  $\alpha$ 's to be tested. A range of  $\alpha$ 's from negative one to three degrees was selected. This set of angles is within the drag bucket at all the selected Reynolds numbers, because these angles fall within the desired operating range they are

of particular interest in terms of influencing performance. Although high yaw angles, close to stall, will certainly produce the highest deflections, accurately capturing the physical conditions occurring near stall is difficult; additionally, AC 50 catamarans typically operate between -1 degrees and 3 degrees of yaw. For these reason, only the lower end of the possible range of yaw angles was tested (Figure 8).

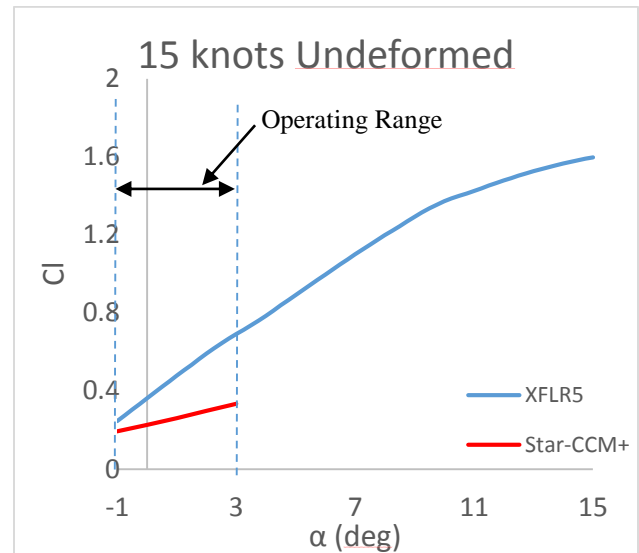


Figure 8 Comparison of Testing Matrix

The final testing matrix is shown below in Figure 9 along with a visualization of the parameters varied. The geometry was tested at three different Reynolds numbers over a range of angles of attack from negative one to three degrees. Vertical lift, drag, and side force were then recorded and compared for both the deformed and undeformed cases. To set the angle of attack, the geometry was rotated about the z-axis. This simulates a change in leeway angle, or yaw, of the vessel. This axis of rotation was selected to induce the maximum possible deflection. All tests were run at an immersion ratio of one to further increase loading.

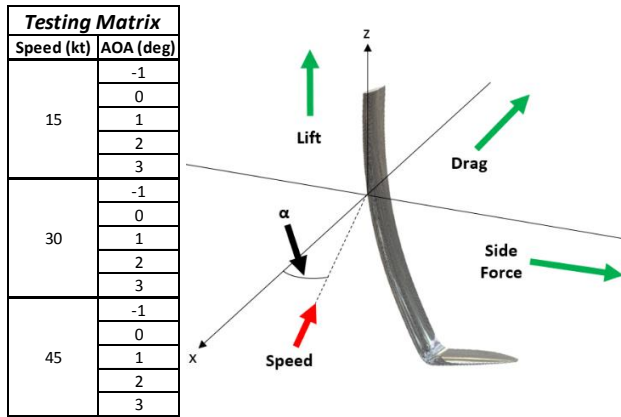


Figure 9 Testing Matrix

### 6.3 SELECTION OF CAE PLATFORM

#### 6.3.1 Star CCM+

Two codes have to be selected for use in a FSI analysis, a CFD code and an FEA code. Modern CAE software often has these codes integrated under one platform but the robustness of the solvers within each platform varies. From the onset it was clear that CD Adapco's Star CCM+ would be the most practical code to use for our CFD analysis. CD Adapco's (Computational Dynamics-Analysis & Design Application Company Ltd) is a multinational CAE computer software company best known for their CFD products. Additionally, Star CCM+ has been used in previous Webb theses, which provided a baseline procedure for performing marine hydrodynamic analysis.

This left the selection of an FEA solver. Early in the selection process the capability to model orthotropic materials was a consideration in this selection. Out of the solvers available for educational use, two in particular were considered; NEi Nastran and Abaqus. Both of these solvers have the capability to run full FEA on complex composite structures. In the case of NEi Nastran, only file based coupling is possible, which, if used, would effectively limit the FSI analysis to a weak coupling. Abaqus, on the other hand, is a full CAE package and not only has the capability to model composite structures, but is also capable of running FSI co-simulation within itself or coupling with Star CCM+. The biggest issue with both of these options is the associated learning curve. The time spent learning additional software, in addition to the added complexity of a composite structure, was not feasible within the given time constraints.

With the possibility of composite FEA out of the question, Star CCM+ once again became the obvious choice. Similar to Abaqus, Star CCM+ is a full CAE package with the ability to run multiple solvers in the same environment. Although many engineering problems involve fluid dynamics, the real-world solution often

involves accounting for a wider range of physical phenomena. For this reason, Star CCM+ has the capability to account for a range of physics, including heat transfer, chemical reaction, combustion, solid transport and acoustics. For this analysis, both the CFD and FEA solver could be run in the same environment. This eliminated the need to learn new software and work through any compatibility issues that may occur in the coupling process.

Another significant benefit from the selection of Star CCM+ as our platform is the customer support and knowledge base offered to users. As an educational user of a CD Adapco product users are provided with access to a designated customer support representative and to a large database of previous support cases and best practices which proved to be extremely useful.

CD Adapco frequently releases updates to their products, with a new release of Star CCM+ occurring every four months. Of particular interest to this thesis, the January version 11.02 included a fluid structure coupling model. Although the code previously had the capability to perform a FSI analysis, this model automated the nuances involved in the coupling of the FEA and CFD solvers.

#### 6.3.2 Computational Resources Available at Webb

Webb recently acquired two Dell Precision 7910 Towers. These computers have been tailored for use in CAE simulation applications. The general specifications of the tower units are presented below in Table 3. The primary hardware components of interest are the CPU and RAM. These computers have a large number of processors capable of hyper threading, and a high speed memory system, with enough channels to complement the processors.

Table 3 Couch Lab Resources

Dell Precision Tower 7910		
<b>CPU</b>	Intel Xeon CPU E5-2697 v3	
	Speed	2.60 GHz
	Sockets	2
	Cores	28
	Threads	56
	Scalability	2S

<b>RAM</b>	Installed	192GB
	Speed	2133MHz
	Slots Used	16/16
	Form Factor	DIMM

<b>GPU</b>	NVIDIA Quadro K6000	
------------	---------------------	--

## 6.4 CPU STUDY

In general, the more cores available to perform calculations, the faster a CAE simulation can run. This is not entirely true for parallel processing applications. Above a certain number of cores, the time it takes to exchange data between cores becomes greater than the time it would take to process that same data in a single core. This issue is known as scaling or scalability.

In order to best utilize the resources available for this analysis, a CPU study was conducted. Putting all theory aside, this is the best way to gauge system performance. This study was conducted by running the same CFD simulation file to convergence with a varying number of logical processors. The total time to complete 500 iterations was recorded for each case. Results from this study are shown below in Figure 10. Results indicated little benefit from running simulations on more than 10 cores at a time. With a total of 40 licenses available from CD Adapco, this enabled four simulations to be run simultaneously. This is well within the capacity of one of the two Couch Lab workstations.

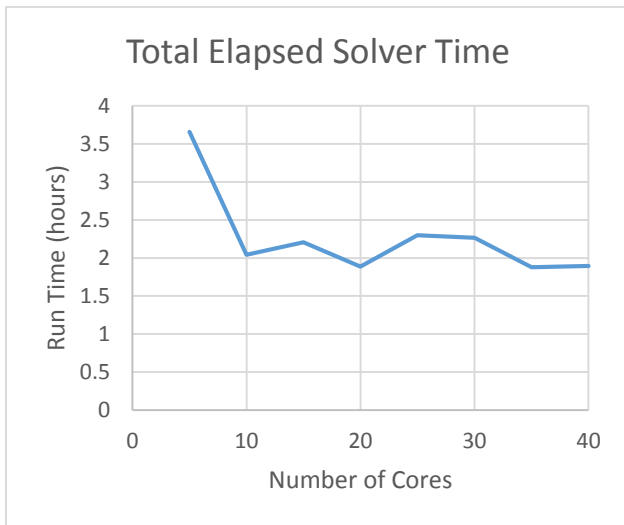


Figure 10 CPU Study Results

## 6.5 COMPUTATIONAL FLUID DYNAMICS

The CFD simulation was first run to convergence independently of the FSI simulation to establish the base characteristics of the undeformed case. This was done for the entire testing matrix. The CFD solution converged after 500 iterations in all cases (Figure 11).

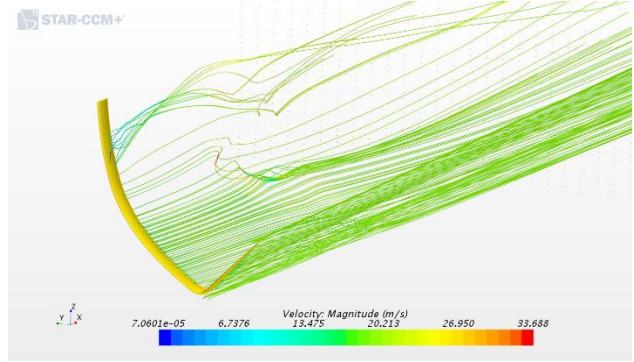


Figure 11 Post processing of CFD solution

### 6.5.1 Geometry

The first step in any multi-physics simulation within StarCCM+ is generating the intended geometry for the study. StarCCM+ has some basic modeling capabilities, but the majority of more complex models will need to be created with a third party CAD program, such as Rhinoceros 3D, which was used for this study. The models can be imported into StarCCM+ using the IGES (Initial Graphics Exchange Specification) format. An important aspect of generating the initial geometry is determining what simplifications, if any, should be applied to the model. This decision should be made based on the computing power available and the level of precision required for design aspects being examined.

A hydrofoil CFD analysis requires the discretization of the foil geometry and the flow domain. The foil geometry is usually imported, while the flow domain can be created in StarCCM+. The flow domain sizing should be large enough to minimize the effect that boundary conditions have on the main region of interest. Adequate flow domain sizing can be established using a mesh sensitivity analysis. This allows an examination of the velocity gradient to ensure that the far field flow is undisturbed by wall effects. It was found that a region sized 16 chord lengths forward and to each side of the foil, 6 chord lengths below, and 40 chord lengths behind the foil was suitable for this simulation (Figure 12).

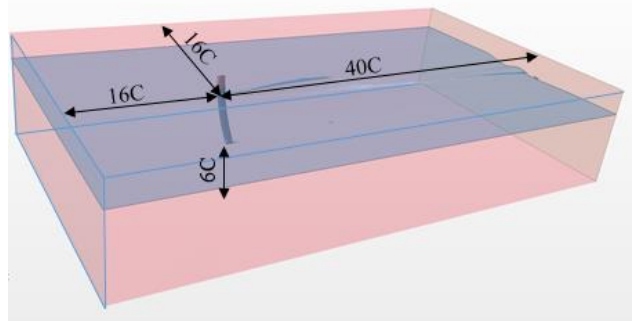


Figure 12 Flow Domain Dimensions

The height of the flow domain above the foil was considered arbitrary as long as it does not affect the free surface, because of the low forces imparted by air in a free surface simulation. Once the two aspects of geometry have been created, the subtract operation can be applied to combine the parts for mesh generation.

### 6.5.2 Meshing

Proper mesh refinement is crucial in any CFD simulation in order to accurately model the physics being simulated. StarCCM+ has a variety of automatic meshes that can be enabled to generate the volume mesh. The surface remesher, trimmed cell mesher, and prism layer mesher were enabled for this simulation. The surface remesher triangulates the geometry mesh to optimize it for inclusion in the volume mesh. The trimmed cell mesher is a robust and efficient way to produce a predominately hexahedral mesh capable of accepting various user-defined refinements. The prism layer mesher is a supplementary volume mesher that generates orthogonal prismatic cells near walls (Figure 13).

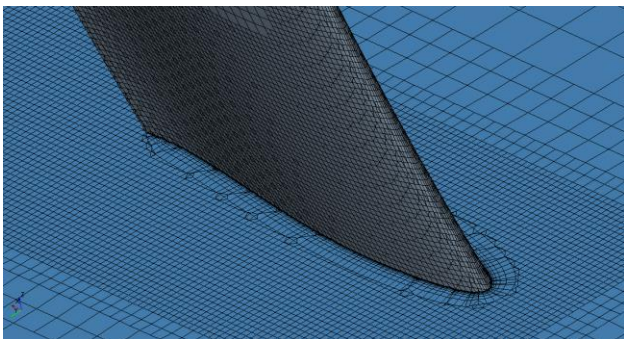
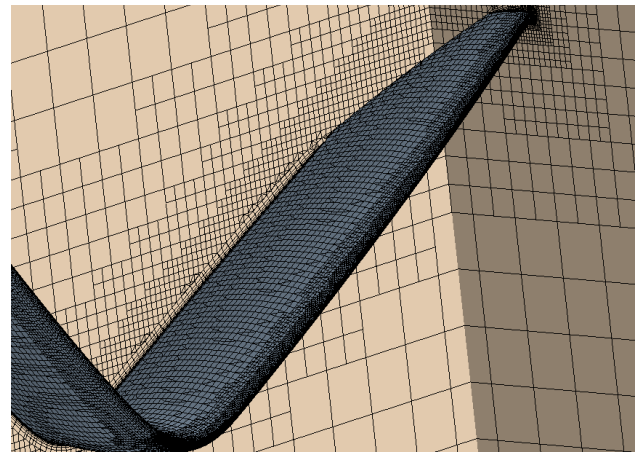


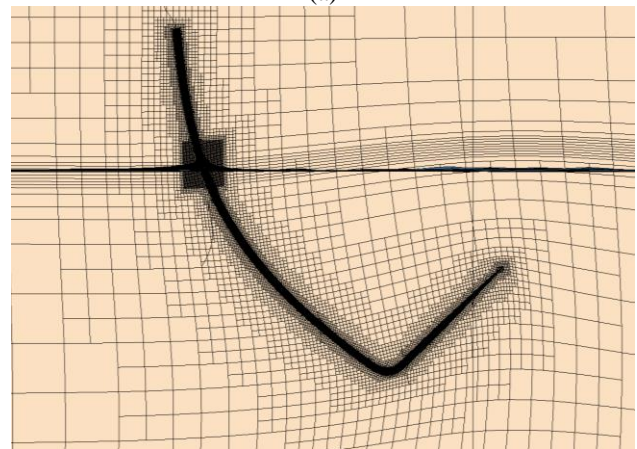
Figure 13 Prism Layer Mesher

The prism layer mesher settings must be applied in conjunction with the turbulence model at the correct  $y^+$  values identified to accurately model the boundary layer.

In addition to the surface and volumetric meshes, StarCCM+ has the ability to add custom mesh refinements. These include volumetric refinements (Figure 14a), surface refinements (Figure 14b), wake refinements and others. Volumetric refinements require additional geometry to be generated for such areas as the free surface and foil ventilation region.



(a)



(b)

Figure 14 (a) Surface Refinements (b) Volumetric Refinements

The wake refinement trimmer (Figure 15) is exceptionally useful in capturing turbulence and vorticity effects downstream of the foil (Figure 16).

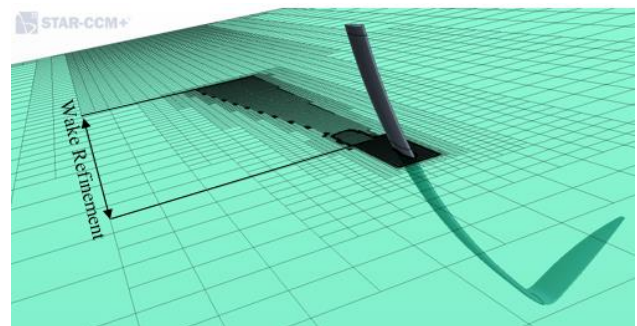


Figure 15 Wake Refinement

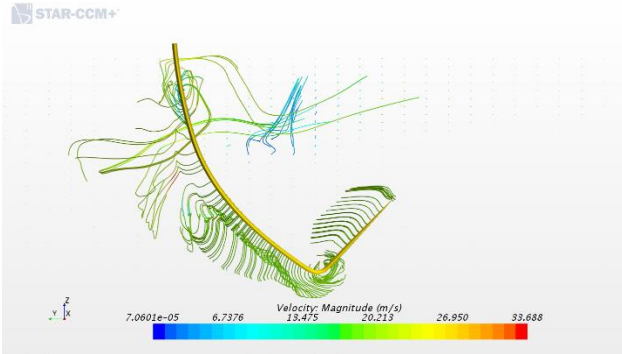


Figure 16 Turbulence Effects

This geometry does not have to be included in the subtract part that represents the extent of the volume mesh, but can be referenced specifically in the mesh custom controls. Surface refinements need to be applied in areas of complex geometry to ensure that mesh simplification does not alter the flow characteristics. Wake regions can be applied to custom surface controls to generate a region of specific size, angle, and refinement relative to a part being analyzed. Once the mesh settings have been applied, the mesh can be generated.

### 6.5.3 Physics

StarCCM+ offers an extensive range of physics models that can be applied to the simulation continua. The physics models selected apply the proper settings for the intended simulation including single/multiphase flow, heat transfer, solid stress, and aeroacoustics among others. The settings applied dictate the simulation physics within the continua. Various physics options also enable the solvers necessary to converge on that type of solution. Of particular note for this analysis are models including Reynolds-Averaged Navier Stokes,  $k-\varepsilon$  turbulence, Volume of Fluid, and Eulerian Multiphase. The Reynolds-Averaged Navier Stokes model enables the equations of the same name, described previously in the theory section; these equations consist of the fundamental underlying equations used to govern fluid flow in this simulation. The  $k-\varepsilon$  turbulence model and its subsequent sub-models are necessary to properly model the turbulent boundary layer flow. The Volume of Fluid model, the Eulerian Multiphase model, along with their respective sub-models, are necessary to model the free surface condition.

### 6.5.4 Regions

Regions are defined as the connection between the geometric side, and physical. The subtract part generated for the flow domain must be assigned to a region prior to generating the mesh, this links the mesh to the appropriate region. The region must then have the proper physics continua applied to it. Regions are used to apply boundary conditions to the problem. The three main

boundary conditions for a foil CFD simulation are velocity inlet, pressure outlet, and wall. A velocity inlet is assigned the velocity and angle of the current operating condition being evaluated; in this simulation the front face and the four sides of the flow domain are selected to be velocity inlets. The pressure outlet is assigned the pressure conditions on the outlet face, in this case the back wall of the flow domain. The wall boundary condition is assigned to all parts being analyzed in the simulation, this condition allows shear forces and pressures to be evaluated.

## 6.6 FINITE ELEMENT ANALYSIS

### 6.6.1 Geometry

Solid stress simulations within StarCCM+ required only the volume of the solid part being analyzed. This can be modeled in a third party CAD software and imported as an IGES file containing the part surfaces. Similar to CFD simulations, the geometry should be carefully refined to balance the computational resources necessary, with the precision level required for the solution being attained.

### 6.6.2 Meshing

Mesh refinement is crucial for attaining accurate FEA results as it is for an accurate CFD solution. FE mesh refinement is not as critical as the CFD mesh discretization, which requires precise definition for results to be considered accurate (Schwer, 2008). A FE mesh typically features fewer cells than a comparative CFD mesh; in this study the FEA mesh consisted of 1 million cells as compared to the CFD mesh which contains over 6 million cells. The most course mesh settings determined to produce the same displacement as the theoretical validation in a cantilevered beam case were applied to the foil FE mesh.

### 6.6.3 Physics

The physics models are chosen in the same manner as the CFD simulation, with implementation of solid stress physics as opposed to fluid flow physics. The main physics model enabled for FEM simulations is the Linear Isotropic Elastic model. This is currently the only form of FEA available within StarCCM+. The isotropic material is also assigned in the physics continua. This is selected under the Solid Model node; for this simulation Aluminum with a Young's Modulus of 68 GPA was assigned as the material. Additional material properties are provided in Table 4.

Table 4 Aluminum Material Properties

Density	2702 kg/m <sup>3</sup>
Poisson's Ratio	0.33
Young's Modulus	68000 MPa

The Linear Isotropic Elastic model within StarCCM+ only models elastic loading, which means an elastic process with no yield stress limit. The stresses encountered in this study, at the highest speeds, actually exceed the yield stress of aluminum, which is why the majority of actual vertical-lift-producing daggerboards are constructed from orthotropic carbon fiber.

#### 6.6.4 Regions

The regions act in nearly the same manner for FE simulations as for CFD simulations. The parts must first be applied to a region before meshing. Within the regions node, the boundary conditions are applied as segments rather than setting the boundary type. The segments applied include fixed constraints at the top and bottom of the daggerboard trunks, where in typical high performance sailing craft, plastic bushings are installed to allow for daggerboards with different foil sections to be installed.

### 6.7 FLUID STRUCTURE INTERACTION

FSI procedure consists of the method of coupling the CFD and FEM simulations into one. This involves interfacing the two models to converge upon a deformed solution. The mesh, physics, and regions from each can be generated from the same foil geometry in a single simulation file. First the CFD simulation is run on its own to convergence at 500 iterations, set by the stopping criteria, with the FE stress solver frozen. At this point the FE model is coupled with the CFD model through the process depicted in the following section on interfacing, the FE stress solver is unfrozen, and the resultant FSI simulation is run for another 500 iterations to convergence.

#### 6.7.1 Interfacing

Once the CFD and FEA simulations have been completed independently, the rest of the FSI model relies on the coupling of the two. This is accomplished through the use of interfaces in StarCCM+. A couple key operations are necessary to interface the two models. The Fluid Structure Coupling model must be enabled in the solid physics continua. The interface can be generated by multi selecting the two regions and creating an interface between the two. The subtract surfaces from the CFD geometry and the respective part surfaces from FE geometry can be multi selected to create a contact between them. The contacts need to be selected under the interface in order for the solver to run.

#### 6.7.2 Solving

Once the steady, undeformed, solution has developed, the FE solver can be unfrozen and the solution of the FSI problem begins. From this point until the end of the simulation each iteration involves the solution of both the fluid and solid solver. Shown below in

Figure 17 is a visual representation of a two-way FSI algorithm.

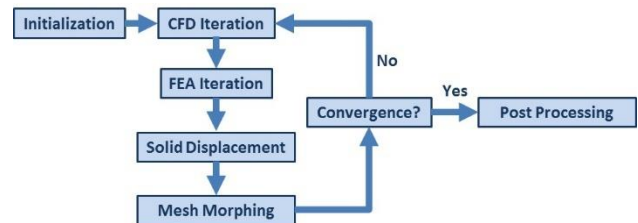


Figure 17 Two-way FSI algorithm

Once both solvers are initialized a CFD iteration is complete. In co-simulation this first “micro” iteration is known as the leading simulation. The CFD solver produces pressure gradients and traction fields which are then applied as loading conditions to the FE model. The FE model then solves the stiffness matrix for nodal displacements. These displacements are then used by the mesh morpher which distorts the existing CFD mesh to match the solid displacement. A depiction of the displaced FE mesh and morphed CFD mesh can be seen in Figure 18. This process is repeated each iteration until convergence is achieved.

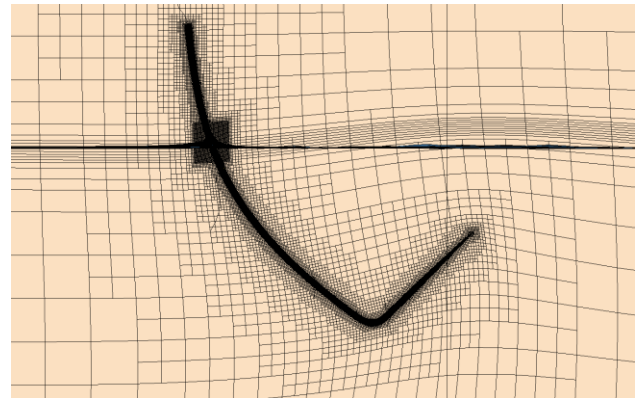


Figure 18 Mesh Morphing

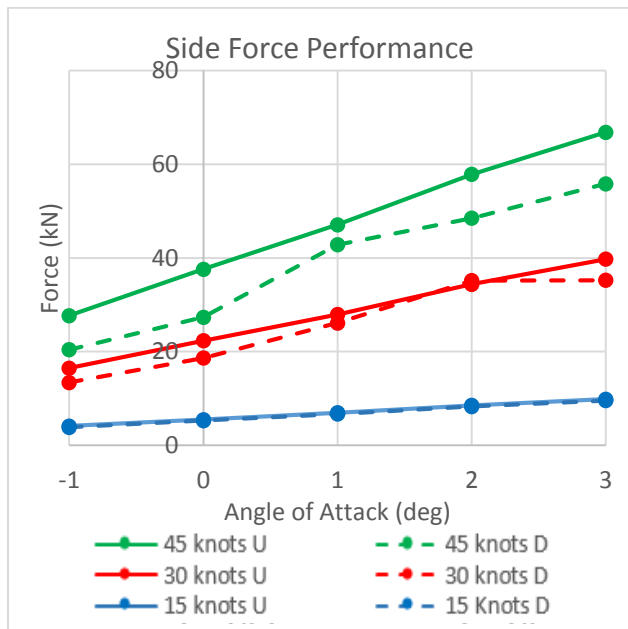
### 6.8 INITIAL CFD SIMULATION

Initial testing consisted of running a series of Star CCM+ environments provided to us by Nate Fast, and running the same foils and testing conditions in the environment that we generated. We compared three yaw angles on the 40-degree tip angle foil and one yaw angle on each of the zero and 20-degree tip angle foils. The results produced in the environment created in the early

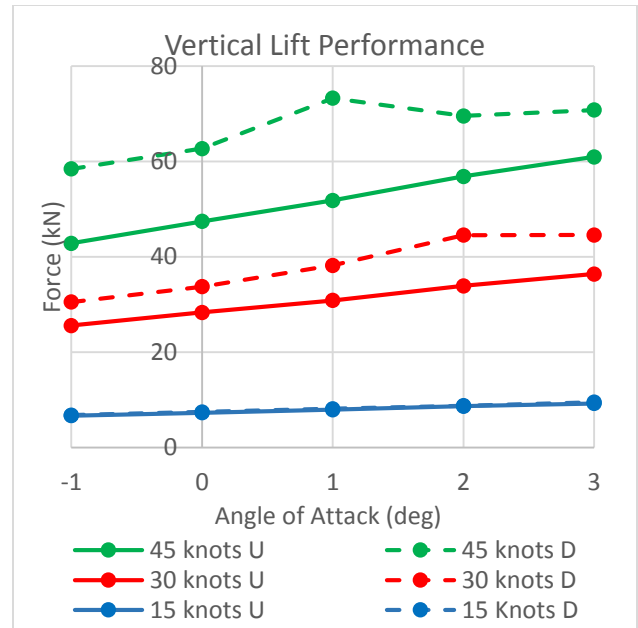
stages of this thesis were compared to the published results in the Fast (2014) thesis and with the results produced by the Fast simulation files. Overall results from the environment we generated were within ten percent of Fast's published results. This was a form of validation of the Star CCM+ procedure being carried out in the initial stages. This exercise also helped with the familiarization of Star CCM+ and its workflow. The results from this validation can be seen in

## 7 RESULTS

Testing was completed for both the undeformed foil, with a solely CFD simulation, and for the deformed foil, with coupled CFD and FEA within StarCCM+, over the entire testing range. The undeformed results show increasing vertical lift, sideforce, and drag with increasing  $\alpha$  and faster operating speeds. This increase in lift and sideforce can be attributed primarily to the lower pressure developed on the suction side the foil at higher speeds. The variations in deformed foil performance from the undeformed case are presented below.



(a)



(b)

Figure 23 Side Force Results (a) and Vertical Lift (b)

The deformed case at 15 knots had very little variation in lift generated between the undeformed and deformed cases. This correlates with the smaller forces produced at the lowest tested operating speed of 15 knots.

As the foil begins to deform, the projected area in the lateral plane, roughly proportional to the sideforce produced, decreases, while the vertical area, likewise proportional to vertical lift, increases. The findings at both 30 and 45 knots show a decrease in sideforce and an increase in lift in the deformed case. This agrees with the expected results from the variance in projected area. The highest operating speed of 45 knots produced the most significant changes in deformed performance. An interesting point to note in the results graph is where the sideforce increases, for the deformed case, at 30 knots and 2 degrees angle of attack. This does not correlate with the change in projected area. Further investigation is needed to determine the cause and possible benefit in that operating region.

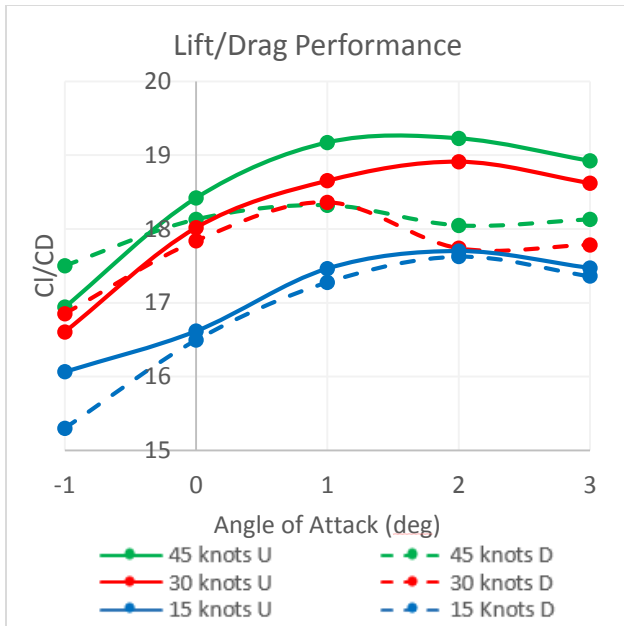


Figure 19 Lift/Drag Performance Results

The lift to drag ratio was established using the total resultant force of the vertical lift and sideforce generated and the expanded area as the reference area. The lift to drag performance throughout the testing matrix can be seen in Figure 19. Once again, at 15 knots, the performance varied little from the undeformed to deformed case. The 30 and 45 knot cases were found to have significant decreases in lift to drag ratio at angles of attack of over 2 degrees from the undeformed case to the deformed case.

A wide variety of results are contained within the FSI solution achieved as the focus of this thesis. Shown in Figure 20 is the change in pressure gradient from negative one to three degrees angle of attack.

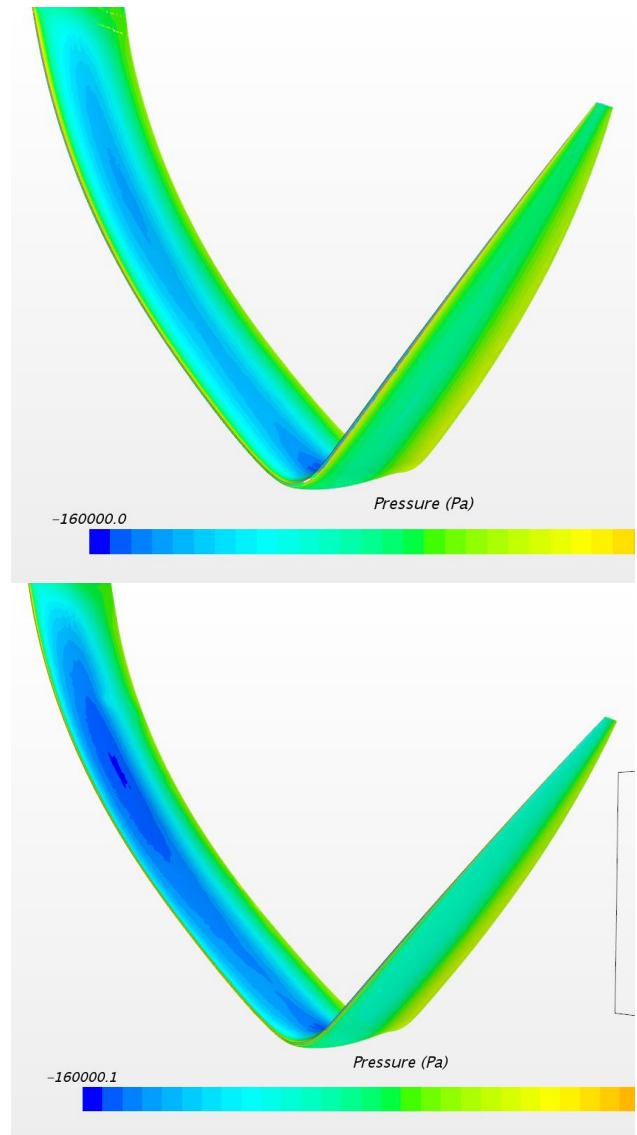


Figure 20 Pressure gradient developed at  $-1^\circ \alpha$  and  $3^\circ \alpha$  at 45kts respectively

The deformation correlated with a cantilevered beam, with a maximum deflection at the tip of the foil. The difference in deflections as a result of varying angle of attack can be seen in Figure 21.

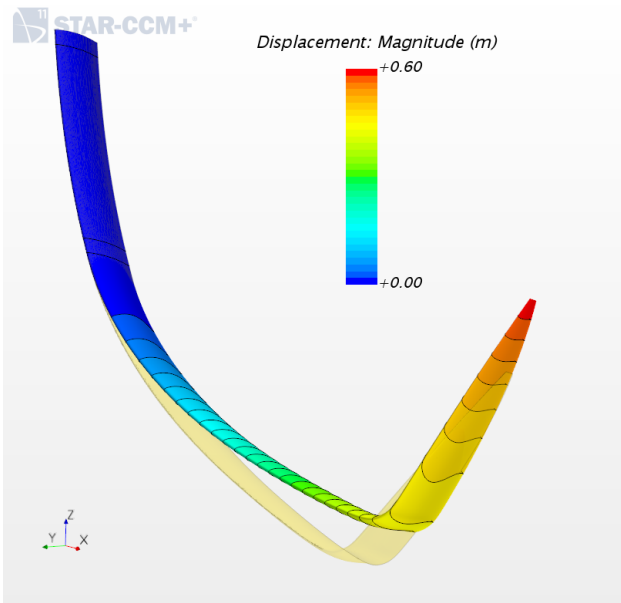
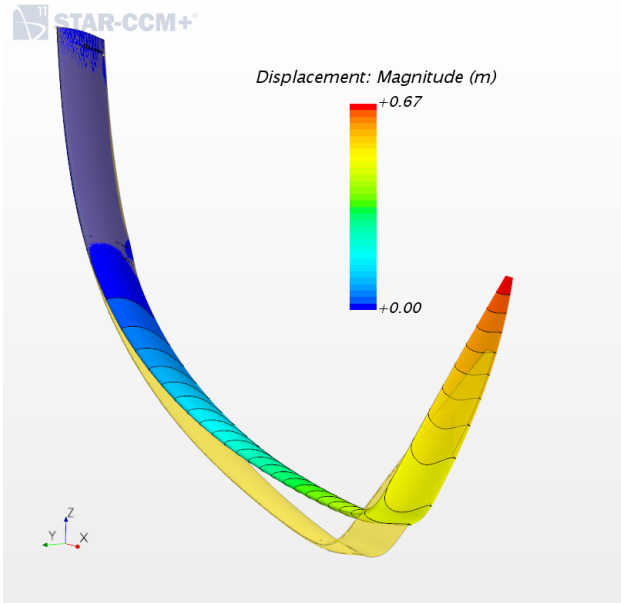


Figure 21 Displacement at  $-1^\circ$  and  $3^\circ \alpha$  at 45kts respectively

Likewise, the stresses reached a maximum at the fixed constraint of the daggerboard trunk (Figure 22), on the low pressure inboard side of the foil, farther from the neutral axis. The aluminum's ultimate yield strength was exceeded in some of the higher loading conditions.

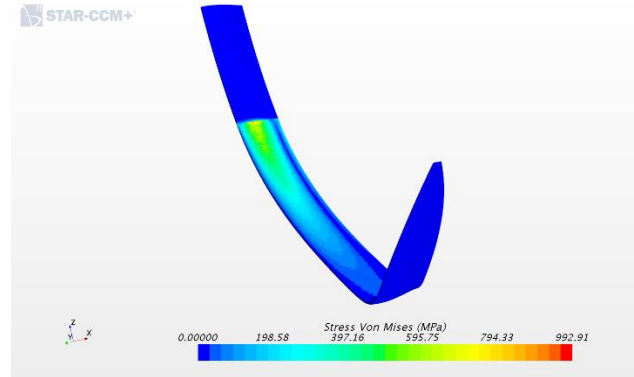


Figure 22 Von Mises Stress at 45kts,  $3^\circ \alpha$

## 8 CONCLUSION

The main objective of this thesis is to couple a CFD analysis and a FE analysis, in order to complete a FSI study of a C-V hydrofoil. A powerful fluid structure interaction analysis procedure was created within the Star-CCM+ environment. The simulation created was tested through a variety of operating conditions, and provided results that can be useful in a preliminary analysis with promising results. Vertical-lift and side-force results follow deformed changes in projected area as expected. Although validation with experimental data is difficult to perform due to the proprietary nature of this work, it is a first step forward in understanding the difference between a pure CFD analysis and FSI analysis.

A secondary goal of this thesis is to evaluate the necessity of considering fluid structure interactions through comparison of a non-deformable CFD analysis to the FSI results. Deformation was found to significantly impact foil performance at speeds of 30 knots and above. As boats using these foils typically operate in the 40 knot plus range, the necessity of including this form of analysis for America's Cup boats and other high speed foiling craft is apparent. Boats that use non-vertical-lift-producing daggerboards, and do not exceed 15 knots, would likely not benefit greatly from this type of analysis.

## 9 LIST OF REFERENCES

- Abbot, Ira H. and Albert E. von Doenhoff. Theory of Wing Sections. New York: Dover Publications, 1959.
- Fast, Nathan. A Computational Fluid Dynamics Analysis of Vertical-Lift-Producing Daggerboards for High-Performance Sailing Yachts. Glen Cove: Webb Institute, 2014.
- Glauert, H. The Elements of Aerofoil and Airscrew Theory. Cambridge, UK: University Press, 1959.
- Munson, B., D. Young and T. Okiishi. Fundamentals of Fluid Mechanics. Hoboken: John Wiley & Sons, 2006.

Schacht, Roxanne and Doug Zangre. A Computational Fluid Dynamics Analysis of Curved Daggerboards on High Performance Sailing Yachts. Glen Cove: Webb Institute, 2013.

Schwer, Leonard E. Is Your Mesh Refined Enough? Estimating Discretization Error using GCI. California: Schwer Engineering & Consulting Services, 2008.

## 10 ACKNOWLEDGEMENTS

We would like to begin by thanking our principal advisor, Professor Adrain S. Onas for his enthusiasm throughout this project. We would also like to thank Pete Melvin at Morrelli and Melvin Design and Engineering for providing the AC50 foil geometry used in this analysis. Thanks also to Tim Yen at CD Adapco who provided extremely valuable support and direction in the use of Star CCM+.

---

**Casey P. Brown**

[Cbrown16@webb.edu](mailto:Cbrown16@webb.edu)

1(401)523.4920

**Cody B. Stansky**

[Cstansky16@webb.edu](mailto:Cstansky16@webb.edu)

1(561)339.9812